Journal of Mathematical Modeling
Vol. 14, No. 2, 2026, pp. 431-451. Research Article

JMM

Hunting cooperation in prey-predator models: spatiotemporal patterns and bifurcation analysis with holling type IV response

Atish Kumar Sethy, Jyotiska Datta*

Department of Mathematics, Central University of Odisha, India

Email(s): atish_phd@cuo.ac.in, jdatta@cuo.ac.in

Abstract. This study examines a class of predator models that incorporate cooperative predation within specialized carnivore populations. The functional response is parameterized, and numerical simulations are employed to support the analytical investigation of pattern formation potential. The principal finding of this work is that stable Turing patterns, such as stripes, can emerge when predator distributions are more localized than those of their prey. Specialized predator groups that cooperate in hunting contribute to the formation of prey aggregation zones (roost patches), as cooperation enhances predation efficiency. The results demonstrate that although predators exhibit limited mobility, cooperative behavior during hunting promotes both successful predation and long-term coexistence with prey populations. *Keywords*:

Predation cooperation, basin of attraction, limit cycle, turing pattern, global stability.
AMS Subject Classification 2010: 34C23, 70K05, 37M10, 34D23.

1 Introduction

Since the publication of Alan Turing's seminal paper on chemical morphogenesis, reaction-diffusion systems have been extensively studied for their role in the emergence of spatial and temporal patterns [18]. A wide variety of physical, chemical, and biological systems exhibit such natural pattern formations. Many of these patterns have been quantitatively described using mathematical models of reaction-diffusion systems [6, 12, 19]. For example, spiral waves typically emerge near the Hopf bifurcation threshold, particularly when the diffusion rate is low. These structures arise from homogeneous oscillations that become unstable under slight perturbations, giving rise to spiral patterns.

Target patterns have also been investigated using diverse analytical and numerical methods [10, 17]. However, it is relatively uncommon for such analytical results to be thoroughly supported by numerical

*Corresponding author
Received: 30 July 2025/ Revised: 6 November 2025/ Accepted: 6 November 2025
DOI: 10.22124/jmm.2025.31303.2805

simulations [5]. The multiscale perturbation approach has frequently been employed to explore the specific conditions under which these patterns emerge. Targets in coupled reaction-diffusion systems tend to form near the intersection of Turing and temporal Hopf bifurcation regions. The derivation of amplitude equations and subsequent stability analyses, as demonstrated by [3,8,14,20], has significantly enhanced our understanding of the mechanisms underlying target pattern formation. These studies are further strengthened by computational simulations that validate the theoretical predictions.

In spatiotemporal predator-prey systems, combinations of patterns—such as stripes—have been reported [2]. According to Gurney et al., stripes can form in the spatial Rosenzweig–MacArthur model. Malchow et al. [11] investigated spiral development in a phytoplankton–zooplankton–fish model using numerical simulations. Medvinsky et al. [11] also explored the emergence of stripes in plankton–fish interaction models, noting that initial formations may eventually disintegrate due to spatiotemporal dynamics. Sherratt et al. [16] highlighted how geographic barriers and landscape size can influence the development of target patterns. Although identifying the precise conditions for the formation of spiral or target patterns in reaction-diffusion systems is challenging, studies like [3] provide valuable guidance. Collectively, these analytical and numerical studies effectively capture the spatiotemporal dynamics inherent in predator-prey systems.

Prey–predator models serve as essential ecological tools for capturing complex population dynamics while accounting for environmental factors and species interactions [6]. Population growth rates can vary across communities due to factors such as asynchronous reproductive timing, skewed sex ratios, reduced foraging or predator avoidance efficiency, inbreeding depression, and group-size effects on fertility. These factors suggest that population density can significantly impact fitness-related traits. When population density falls below a certain threshold, it may lead to reduced reproductive success and eventual decline [6].

Cooperative predation is a critical factor in predator-prey interactions that must be considered in ecological models. Many predators form groups to increase hunting efficiency [7]. Examples include coyotes, jackals, lions, wolves, spotted hyenas, and dolphins, as well as avian species such as Harris's hawk and several shrikes and kookaburra species. Cooperative predation is also observed in reptiles and fish on rare occasions. This coordinated behaviour can be modelled using game-theoretic approaches or differential equations that account for predator group size, number of prey, and predation success. Alves and Hilker proposed a model using two ordinary differential equations to describe pack predation, introducing a cooperation term to study coexistence and bifurcation properties [1]. While these models offer insight into predator cooperation, few reaction-diffusion models have explicitly incorporated cooperative predation. Furthermore, the role of predation cooperation in spatial and spatiotemporal pattern formation remains underexplored.

Thus, this study aims to investigate how cooperative predation influences pattern formation in predator–prey models. We demonstrate that, under appropriate initial conditions, stripe patterns can emerge. Using multiscale perturbation techniques, we derive the linear amplitude equations and verify our analytical predictions through numerical simulations.

The article is organised as follows: Sections 2, 3, and 4 discuss the relevant spatiotemporal model, along with the existence of steady points, positivity conditions, and local and global stability analysis. Section 5 covers the corresponding model, along with bifurcation requirements. The stability of limit cycles and spatial Turing derivation is addressed in Sections 6, 7, and 8, while the numerical validation of the analytical results is presented in Section 9. Finally, the discussion and conclusion are provided in Section 10.

Table 1: The meaning of the parameter for system (1)

Parameter	Representaion
K	The carrying capacity for prey.
m	The predator's natural rate of mortality.
r	Prey's intrinsic growth rate.
e	Efficiency of conversion.

2 The model

The prey-predator model, which incorporates consumers at multiple trophic levels that function both as prey and predators within a food web, serves as the fundamental building block for understanding complex ecological networks. These models, represented by a set of ordinary differential equations, offer valuable insights into the broader dynamics of prey-predator interactions within biological systems. As such, they have become the focus of extensive research. By examining the dynamics and behavioural responses within these models, we can gain a deeper understanding of various ecological phenomena. The traditional Lotka-Volterra or Gause prey-predator models have long served as the foundation for such studies, but modern variations of these models often build upon or modify these classic formulations. These updated paradigms aim to reflect more accurately the complexities of real-world ecosystems, incorporating additional factors such as resource availability, environmental conditions, or multi-species interactions. In many cases, the newer models share a similar structure to their predecessors but offer improvements or refinements that enhance their applicability and predictive power. Let us now consider a system that incorporates,

$$\frac{du}{dT} = ru\left(1-\frac{u}{k}\right) - \phi(u,v)v, \tag{1a}$$

$$\frac{dv}{dT} = e\phi(u,v)v - mv. \tag{1b}$$

Initiall conditions are $u(0) > 0, v(0) > 0$, $u \equiv u(T)$ and $v \equiv v(T)$, and all positive parameters are displayed in the Table 1, where $u(T)$ and $v(T)$ are the densities of prey and predator populations at time T, respectively.

Additionally, $\phi(u,v)$ denotes the frequency at which each predator kills prey, which is the overall functional response of predators to prey. The ratio of prey to predators might play a role.

If the functional response $\phi(u)$ depends solely on prey density, it is referred to as prey-dependent. This implies that the rate at which a predator consumes prey is entirely determined by the abundance of the prey population. One of the simplest forms of prey-dependent functional responses is the linear response, found in the classical Lotka–Volterra model, and defined by $\phi(u) = \lambda u$, commonly known as Holling Type I. In this case, the predation rate increases proportionally with prey density, where λ is a constant representing the predator's encounter or capture efficiency. This form assumes no handling time and implies that predators have unlimited appetite, which may not be realistic in most ecological settings. More ecologically realistic dynamics are captured by Holling Type II, given by $\phi(u) = \frac{\lambda u}{c+u}$, where c represents the half-saturation constant. This formulation introduces the concept of handling time—the time a predator spends capturing, killing, and consuming prey. As prey density increases, the predation rate rises but eventually levels off, approaching a maximum rate due to the predator's limited capacity to pro-

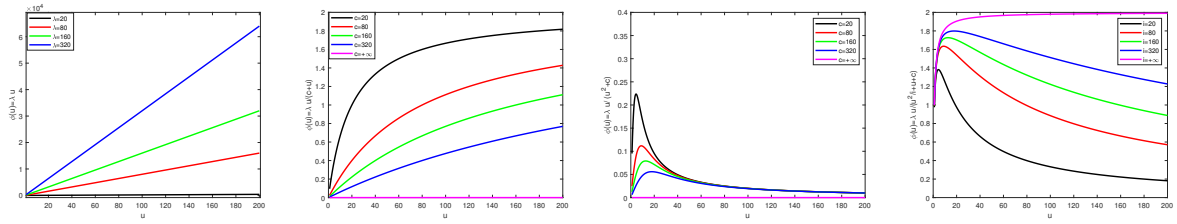

(a) **(b)** **(c)** **(d)**

Figure 1: Diagram depicts the Holling type-I, II, III, IV functinal response.

cess additional prey. This response is common in systems where predators become satiated and cannot continue increasing their consumption indefinitely. Holling Type III, described by $\phi(u) = \frac{\lambda u}{c+u^2}$, adds further ecological realism by incorporating a sigmoidal response. At low prey densities, the predation rate increases slowly, possibly due to prey hiding more effectively or predators taking longer to locate prey. As prey become more abundant, predation accelerates, before again levelling off at higher densities due to saturation. This form captures phenomena such as learning behaviour in predators and prey refuges, and is often observed in natural ecosystems where prey switching or alternative food sources exist. Finally, Holling Type IV, represented by $\phi(u) = \frac{\lambda u}{\frac{u^2}{i}+u+c}$, introduces a dome-shaped response. Here, predation increases with prey density up to a certain threshold but then declines at very high prey densities. This may occur due to predator confusion, interference, or reduced efficiency in densely packed prey populations. Parameters i and c help shape the curvature of the response. This functional form is particularly useful in modelling scenarios involving cooperative predation or when predator efficiency is hindered by overcrowding or complex spatial interactions among prey. Figure 1 presents the numerical representations of all types of functional responses. The density of the target and predator populations may affect $\phi(u,v)$ like ratio-dependent reactions and functional responses according to Crowley-Martin, Beddington-DeAngelis, etc.

However, when predation incorporates cooperative behaviour, both prey and predator densities become essential in determining the functional response $\phi(u,v)$. In such cases, the rate of prey capture increases with rising predator density. This assumption can be modelled by introducing a predator density-dependent term into the capture rate, such as $\lambda + a_1 v$ [13], where $a_1 > 0$ quantifies the degree of cooperation among predators during hunting. Consequently, the functional response changes from $\phi(u,v)$ to $\phi(u,\lambda + a_1 v)$, thereby introducing predator dependence into the formulation. When $a_1 = 0$, the model reduces to a classical prey-dependent framework, where only prey density influences the functional response. This approach was employed by Alves and Hilker, inspired by the methodology proposed by Berec [3], to incorporate the cooperative predation term in its simplest form. A commonly used representation of cooperative predation within a prey–predator framework is given by the following Holling type IV functional response:

$$\phi(u,\lambda + a_1 v) = \frac{u(\lambda + a_1 v)}{\frac{u^2}{i} + u + c},$$

as described in [13]. This captures a dome-shaped response, where predation increases with prey density up to a point, and then declines at very high prey densities due to interference or reduced efficiency.

The corresponding model is formulated as:

$$\frac{du}{dT} = ru\left(1-\frac{u}{k}\right) - \frac{uv(\lambda + a_1 v)}{\frac{u^2}{i} + u + c}, \tag{2a}$$

$$\frac{dv}{dT} = e\frac{u(\lambda + a_1 v)}{\frac{u^2}{i} + u + c}v - mv. \tag{2b}$$

We start with $\xi_1 = \frac{eu}{m}$, $\xi_2 = \frac{ev}{m}$, $t = mT$, $s = \frac{r}{m}$, $L = \frac{ke}{m}$, $b = \frac{\lambda e}{m}$, $g = \frac{a_1 m}{\lambda}$, $a = \frac{ie}{m}$ and $d = \frac{ce}{m}$. We get the non-dimensional form of the system, which is

$$\frac{d\xi_1}{dt} = s\xi_1\left(1-\frac{\xi_1}{L}\right) - \frac{b(1+g\xi_2)\xi_1\xi_2}{\frac{\xi_1^2}{a} + \xi_1 + d}, \tag{3a}$$

$$\frac{d\xi_2}{dt} = \frac{b(1+g\xi_2)\xi_1\xi_2}{\frac{\xi_1^2}{a} + \xi_1 + d} - \xi_2. \tag{3b}$$

The parameters of systems (3) are positive and dimensionless variables. For these equations, the non-negative initial conditions are $\xi_1(0) \geq 0$, and $\xi_2(0) \geq 0$.

3 Existence of steady states

We shall identify the model's equilibrium point by analysing the related characteristics equations for the model under consideration $\phi_1(\xi_1, \xi_2) = 0$ and $\phi_2(\xi_1, \xi_2) = 0$ i.e.

$$s\xi_1\left(1-\frac{\xi_1}{L}\right) - \frac{b(1+g\xi_2)\xi_1\xi_2}{\frac{\xi_1^2}{a} + \xi_1 + d} = 0, \tag{4a}$$

$$\frac{b(1+g\xi_2)\xi_1\xi_2}{\frac{\xi_1^2}{a} + \xi_1 + d} - \xi_2 = 0. \tag{4b}$$

We obtain the positive axis steady point by solving the given system, which is $E_1(0,0)$ and $E_2(L,0)$. The significant prey and predator nullclines of the model (3) are

$$\xi_1 = (1+g\xi_2^*)\xi_1^* - \frac{\xi_1^{2*}}{a} - d, \xi_2 = s * \xi_1^*(1-\frac{\xi_1^*}{L}),$$

respectively. Using the value of ξ_2 from the predators' nullcline equations into prey nullclines, we can derive a cubic equation of ξ_1 as follows:

$$f(\xi_1) \equiv \frac{gb}{dL}\xi_1^3 - \frac{1}{d}(gb - \frac{1}{g})\xi_1^2 - \frac{1}{g}(b-1)\xi_1 + 1 = 0$$

given that $f(-\infty) < 0$ and $f(1) > 0$ from the given expression of $f(\xi_1)$, there must exist at least one root where $g^2 b < 1$ and $b > 1$. Since $f'(\xi_1)$ has two non-negative real parts $(\frac{L(gb-\frac{1}{g})}{3gb} \pm \frac{L\sqrt{(gb-\frac{1}{g})^2 + 3\frac{gb}{L}(b-1)}}{3gb})$, we conclude that $f(\xi_1)$ has at least one negative root, two non-negative the roots, and two non-zero roots. The coexistence equilibrium point (ξ_1^*, ξ_2^*) is determined by the intersection of the prey and predator nullclines, as shown in Figure 2. In Figure 2a, there is a single coexistence equilibrium, while Figure 2b illustrates the existence of two interior equilibrium points.

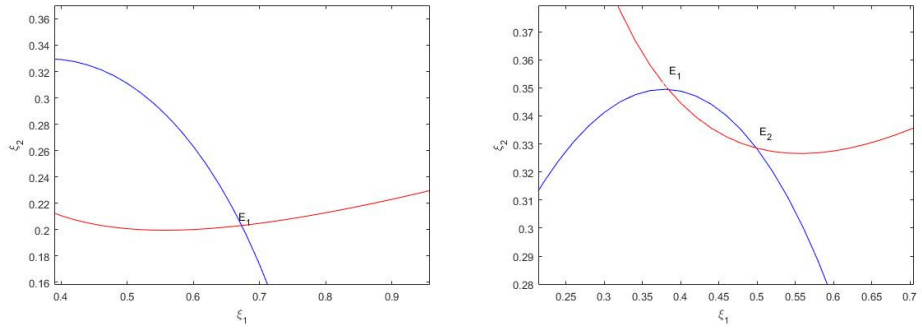

(a) **(b)**

Figure 2: In this diagram, the red colour is for the predator population and the blue is for the prey population functional response nullclines for system (3).

3.1 Positivity of system

Consider

$$\frac{d\xi_1}{dt} = \xi_1\left(s\left(1-\frac{\xi_1}{L}\right) - \frac{b(1+g\xi_2)\xi_2}{\frac{\xi_1^2}{a}+\xi_1+d}\right) = \xi_1\phi_3(\xi_1,\xi_2), \tag{5a}$$

$$\frac{d\xi_2}{dt} = \xi_2\left(\frac{b(1+g\xi_2)\xi_1}{\frac{\xi_1^2}{a}+\xi_1+d} - 1\right) = \xi_2\phi_4(\xi_1,\xi_2), \tag{5b}$$

with the initial conditions $\xi_1(0) = \xi_{10} > 0$ and $\xi_2(0) = \xi_{20} > 0$, and all variables used in the given system are positive. Also,

$$\phi_3(\xi_1,\xi_2) = s\left(1-\frac{\xi_1}{L}\right) - \frac{b(1+g\xi_2)\xi_2}{\frac{\xi_1^2}{a}+\xi_1+d}, \tag{6a}$$

$$\phi_4(\xi_1,\xi_2) = \frac{b(1+g\xi_2)\xi_1}{\frac{\xi_1^2}{a}+\xi_1+d} - 1. \tag{6b}$$

Theorem 1. *Considering the initial circumstances supplied, every solution to system (5) is always positive.*

Proof. We have to show $(\xi_1,\xi_2) \in \mathbb{R}\ \forall \in [0,\infty)$, such that $\xi_1(t) \geq 0$ and $\xi_2(t) \geq 0$. From model (3) we get

$$\xi_1(t) = \xi_{10}e^{\int_0^t \phi_3(\xi_1,\xi_2)d\bar{t}},$$
$$\xi_2(t) = \xi_{20}e^{\int_0^t \phi_4(\xi_1,\xi_2)d\bar{t}}.$$

Since there exists an $M > 0$ such that $\forall t \in [0,\bar{t}]$ is clearly defined and continuous on (ξ_1,ξ_2), we have

$$\xi_1(t) = \xi_{10}e^{\int_0^t \phi_3(\xi_1,\xi_2)d\bar{t}} \geq \xi_{10}e^{M\bar{t}},$$

Table 2: Table for stability analysis at each of the equilibrium/steady points

Steady point	Jacobian matrix	Nature of stability
$E_1(0,0)$	$A_1 = \begin{bmatrix} s & 0 \\ 0 & -1 \end{bmatrix}$	Saddle
$E_2(L,0)$	$A_2 = \begin{bmatrix} -s & -\frac{bL}{\frac{L^2}{a}+L+d} \\ 0 & -1+\frac{bL}{\frac{L^2}{a}+L+d} \end{bmatrix}$	Stable if $\frac{bL}{\frac{L^2}{a}+L+d} < 1$, unstable if $\frac{bL}{\frac{L^2}{a}+L+d} > 1$

$$\xi_2(t) = \xi_{20} e^{\int_0^t \phi_4(\xi_1,\xi_2)d\bar{t}} \geq \xi_{20} e^{M\bar{t}}.$$

From the given expression, we concluded that if $t \to \bar{t}$, we obtain

$$\xi_1(t) = \xi_1(\bar{t}) \geq \xi_{10} e^{M\bar{t}},$$
$$\xi_2(t) = \xi_2(\bar{t}) \geq \xi_{20} e^{M\bar{t}},$$

which contradicts our assumption. Hence, all the solutions related to the given system are always positive. □

4 Stability analysis

Our primary objective is to examine possible solutions for a dynamical system under particular conditions. Ecological stability governs amplitude, consistency, elasticity, resilience, and persistence. The appropriate definition belongs in the environmental context. Dynamical systems introduce the notion of neighbourhood instability and the sphere of attraction of the ecosystem [4, 15]. A system is considered locally stable if it remains stable under minor perturbations and globally stable if it has a single equilibrium point throughout the whole region of attraction. To investigate the stability of its equilibriums, we linearise a mathematical model constructed concerning a specific environment. The Lyapunov stability method is a popular technique for determining the global stability of any mathematical model.

4.1 Local stability analysis

Three non-negative equilibria can occur for model systems: $E_1(0,0)$ (trivial equilibrium point), $E_2(L,0)$ (predator-free/axial equilibrium point), and $E_3(\xi_1^*, \xi_2^*)$ (coexistence/interior equilibrium point). We now show the matching criteria for the coexistence equilibrium point E_3 in Table 2, together with the feasibility and stability requirements for the system's first two equilibria (3). The Jacobian matrix of system (3) appears as follows at each selected equilibrium point:

$$A_3 = \begin{bmatrix} s(1-\frac{2\xi_1^*}{L}) - \frac{b(1+g\xi_2^*)\xi_2^*(d-\frac{\xi_1^{*2}}{a})}{(\frac{\xi_1^{*2}}{a}+\xi_1^*+d)^2} & -\frac{2gb\xi_1^*\xi_2^*+b\xi_1^*}{\frac{\xi_1^{*2}}{a}+\xi_1^*+d} \\ \frac{b(1+g\xi_2^*)\xi_2^*(d-\frac{\xi_1^{*2}}{a})}{(\frac{\xi_1^{*2}}{a}+\xi_1^*+d)^2} & \frac{2gb\xi_1^*\xi_2^*+b\xi_1^*}{\frac{\xi_1^{*2}}{a}+\xi_1^*+d} - 1 \end{bmatrix}.$$

The interior/coexisting equilibrium/steady point exists where

$$\xi_1 = (1+g\xi_2^*)\xi_1^* - \frac{\xi_1^{2*}}{a} - d, \xi_2 = s*\xi_1^*(1-\frac{\xi_1^*}{L}).$$

By using the value of ξ_2 from the predators we can derive a cubic equation of ξ_1, as

$$f(\xi_1) \equiv \frac{gb}{dL}\xi_1^3 - \frac{1}{d}(gb-\frac{1}{g})\xi_1^2 - \frac{1}{g}(b-1)\xi_1 + 1 = 0.$$

Now

$$\begin{aligned} f(0) =& 1 > 0, \\ f(L) =& \frac{1}{gd}L^2 - \frac{1}{g}(b-1)L + 1 < 0 \quad \text{if} \quad g < L(b-1-\frac{L}{d}). \end{aligned}$$

The coexisting equilibrium point $E_3(\xi_1^*, \xi_2^*)$ is indicated by the equation's positive root in $(0, L)$ due to $f(0)f(L) < 0$. The characteristic equation at the equilibrium point $E_3(\xi_1^*, \xi_2^*)$ is as follows:

$$P(\lambda) = \lambda^2 + C_1\lambda + C_2,$$

where $A_3 = \begin{bmatrix} A_{11} & A_{12} \\ A_{21} & A_{22} \end{bmatrix}$ is the Jacobian matrix of the model system (3) at equilibrium point $E_3(\xi_1^*, \xi_2^*)$, and the coefficients are $C_1 = -(A_{11}+A_{22}) = -tr(A)$ and $C_2 = det(A)$. The components of the Jacobian matrix are as follows:

$$\begin{aligned} A_{11} =& s(1-\frac{2\xi_1^*}{L}) - \frac{b(1+g\xi_2^*)\xi_2^*(d-\frac{\xi_1^{*2}}{a})}{(\frac{\xi_1^{*2}}{a}+\xi_1^*+d)^2}, \quad A_{12} = -\frac{2gb\xi_1^*\xi_2^* + b\xi_1^*}{\frac{\xi_1^{*2}}{a}+\xi_1^*+d} \\ A_{21} =& \frac{b(1+g\xi_2^*)\xi_2^*(d-\frac{\xi_1^{*2}}{a})}{(\frac{\xi_1^{*2}}{a}+\xi_1^*+d)^2}, \quad A_{22} = \frac{2gb\xi_1^*\xi_2^* + b\xi_1^*}{\frac{\xi_1^{*2}}{a}+\xi_1^*+d} - 1. \end{aligned}$$

According to the Routh–Hurwitz criteria, if $\text{tr}(A) < 0$ and $\det(A) > 0$, the characteristic polynomial will have either negative real roots or a pair of complex conjugate roots with negative real parts. Therefore, the coexistence equilibrium point $E_3(\xi_1^*, \xi_2^*)$ is locally asymptotically stable if and only if $\text{tr}(A) < 0$, $\det(A) > 0$. These conditions can be expressed as follows:

$$\begin{aligned} & s(1-\frac{2\xi_1^*}{L}) - \frac{b(1+g\xi_2^*)\xi_2^*(d-\frac{\xi_1^{*2}}{a})}{(\frac{\xi_1^{*2}}{a}+\xi_1^*+d)^2} + \frac{2gb\xi_1^*\xi_2^* + b\xi_1^*}{\frac{\xi_1^{*2}}{a}+\xi_1^*+d} - 1 < 0, \\ & \left(s(1-\frac{2\xi_1^*}{L}) - \frac{b(1+g\xi_2^*)\xi_2^*(d-\frac{\xi_1^{*2}}{a})}{(\frac{\xi_1^{*2}}{a}+\xi_1^*+d)^2}\right)\left(\frac{2gb\xi_1^*\xi_2^* + b\xi_1^*}{\frac{\xi_1^{*2}}{a}+\xi_1^*+d} - 1\right) - \\ & \qquad \left(-\frac{2gb\xi_1^*\xi_2^* + b\xi_1^*}{\frac{\xi_1^{*2}}{a}+\xi_1^*+d}\right)\left(\frac{b(1+g\xi_2^*)\xi_2^*(d-\frac{\xi_1^{*2}}{a})}{(\frac{\xi_1^{*2}}{a}+\xi_1^*+d)^2}\right) > 0. \end{aligned}$$

If we simplify the above inequalities, we obtain

$$ab(s(1+\xi_2^*)+\xi_2^*)+\xi_1^* < (2sb\xi_1^*(1+g\xi_2^*)+dL)a,$$
$$d > \frac{\xi_1^{*2}}{a}.$$

Hence, the coexistence equilibrium point $E_3(\xi_1^*, \xi_2^*)$ is locally asymptotically stable whenever the above conditions are satisfied.

4.2 Global stability analysis

Global stability is the ability of a system to return to the equilibrium point from any initial state. A dynamical system's attractive basin of trajectories can be either the state space or a particular area inside the state space that serves as the system's state variables' identifying region. When a system exhibits global stability, it has a single equilibrium point across the whole area of attraction. International stability is one kind of asymptotic stability. The global stability of system (3) is explained below concerning its coexistence equilibrium point, $E_3(\xi_1^*, \xi_2^*)$.

Theorem 2. *The interior equilibrium point $E_3(\xi_1^*, \xi_2^*)$ is globally asymptotically stable if the conditions $b\xi_1^* > \frac{m^2}{a} + m + d$ and $b(1+gM) < 1$ hold where $m < \xi_1, \xi_2 < M$.*

Proof. We define the Lyapunov function as

$$V(\xi_1, \xi_2) = \int_{\xi_1^*}^{\xi_1} \frac{\xi_1 - \xi_1^*}{\xi_1} d\xi_1 + \int_{\xi_2^*}^{\xi_2} \frac{\xi_2 - \xi_2^*}{\xi_2} d\xi_2. \tag{7}$$

Differentiating equation (7) with respect to time along the solution equation (3a) and (3b) and, we obtain

$$\begin{aligned}\frac{dV}{dt} &= \frac{\xi_1 - \xi_1^*}{\xi_1}\frac{d\xi_1}{dt} + \frac{\xi_2 - \xi_2^*}{\xi_2}\frac{d\xi_2}{dt} \\ &= (\xi_1 - \xi_1^*)\left[s\left(1 - \frac{\xi_1}{L}\right) - \frac{b(1+g\xi_2)\xi_2}{\frac{\xi_1^2}{a} + \xi_1 + d}\right] + (\xi_2 - \xi_2^*)\left[\frac{b(1+g\xi_2)\xi_1}{\frac{\xi_1^2}{a} + \xi_1 + d} - 1\right],\end{aligned} \tag{8}$$

Since $\xi_1, \xi_2 < M$, and we assume that $\xi_1, \xi_2 \geq m > 0$ when $t > T$ for some $T > 0$, equation (8) becomes

$$\begin{aligned}\frac{dV}{dt} &< (\xi_1 - \xi_1^*)\left[-\frac{s}{L}(\xi_1 - \xi_1^*) - \frac{b(\xi_2 - \xi_2^*)\xi_2}{\frac{m^2}{a} + m + d} + \xi_2^*\left(\frac{1}{\xi_1^*} - \frac{b}{\frac{m^2}{a} + m + d}\right)\right] \\ &\quad + (\xi_2 - \xi_2^*)\left[b(1+gM) - 1\right], \\ &< -\frac{s}{L}(\xi_1 - \xi_1^*)^2 - \frac{b}{\frac{m^2}{a} + m + d}(\xi_1 - \xi_1^*)(\xi_2 - \xi_2^*) - \xi_2^*\left(\frac{b}{\frac{m^2}{a} + m + d} - \frac{1}{\xi_1^*}\right)(\xi_1 - \xi_1^*) \\ &\quad - (1 - b(1+gM))(\xi_2 - \xi_2^*).\end{aligned}$$

Thus $\frac{dV}{dt} < 0$ under the hypothesis of Theorem 2. Therefore, the coexisting equilibrium point $E_3(\xi_1^*, \xi_2^*)$ is globally asymptotically stable under the given condition of Theorem 2. □

5 Hopf bifurcation

Now we define how the internal steady points $E_3(\xi_1^*, \xi_2^*)$ behave in terms of stability. When $Re\lambda = 0$ and $Im\lambda \neq 0$, the Hopf bifurcation takes place. As a result, the Jacobian matrix linked to $E_3(\xi_1^*, \xi_2^*)$ must have a positive determinant at the Hopf bifurcation and a zero trace. Consequently, we specify the Jacobian matrix

$$A_3 = \begin{bmatrix} A_{11} & A_{12} \\ A_{21} & A_{22} \end{bmatrix},$$

where

$$A_{11} = s(1 - \frac{2\xi_1^*}{L}) - \frac{b(1+g\xi_2^*)\xi_2^*(d - \frac{\xi_1^{*2}}{a})}{(\frac{\xi_1^{*2}}{a} + \xi_1^* + d)^2}, \; A_{12} = -\frac{2gb\xi_1^*\xi_2^* + b\xi_1^*}{\frac{\xi_1^{*2}}{a} + \xi_1^* + d},$$
$$A_{21} = \frac{b(1+g\xi_2^*)\xi_2^*(d - \frac{\xi_1^{*2}}{a})}{(\frac{\xi_1^{*2}}{a} + \xi_1^* + d)^2}, \; A_{22} = \frac{2gb\xi_1^*\xi_2^* + b\xi_1^*}{\frac{\xi_1^{*2}}{a} + \xi_1^* + d} - 1.$$

By solving $tr(A) = 0$, we can get Hopf bifurcation threshold at g as follows:

$$g = \frac{2sb\xi_1^{*3} - s\xi_1^* L(\xi_1^{*2} + \xi_1^* + d) + L\xi_2^*(d - \frac{\xi_1^{*2}}{a})}{\xi_2^*}.$$

Since $tr(A) = 0$, $det(A) > 0$ at g and $\frac{d}{dg}(A_{11} + A_{22}) \neq 0$ at g, this confirms that a Hopf bifurcation occurs near a stable point.

6 Stability of limit cycle

Let us introduce small perturbations to the region surrounding the interior steady state point by setting $\bar{\xi}_1 = \xi_1 - \xi_1^*$ and $\bar{\xi}_2 = \xi_2 - \xi_2^*$. For convenience, we use ξ_1 and ξ_2 instead of $\bar{\xi}_1$ and $\bar{\xi}_2$, respectively. We have

$$\begin{aligned} \frac{d\xi_1}{dt} &= (\xi_1 + \xi_1^*)(1 - \xi_1 - \xi_1^*)\left(\frac{\xi_1 + \xi_1^*}{L} - 1\right) - \frac{b(1+g\xi_2^*)(\xi_1 + \xi_1^*)(\xi_2 + \xi_2^*)}{\frac{(\xi_1+\xi_1^*)^2}{a} + (\xi_1 + \xi_1^*) + g}, \\ \frac{d\xi_2}{dt} &= \frac{b(1+g\xi_2^*)(\xi_1 + \xi_1^*)(\xi_2 + \xi_2^*)}{\frac{(\xi_1+\xi_1^*)^2}{a} + (\xi_1 + \xi_1^*) + g} - d(\xi_2 + \xi_2^*). \end{aligned} \tag{9}$$

The series expression for the system described in equation (9), subject to the condition $i + j > 4$, is derived as follows:

$$\begin{aligned} \frac{d\xi_1}{dt} &= a_{10}\xi_1 + a_{01}\xi_2 + a_{20}\xi_1^2 + a_{11}\xi_1\xi_2 + a_{02}\xi_2^2 + a_{30}\xi_1^3 + a_{21}\xi_1^2 y + a_{03}\xi_2^3 + G^1(\xi_1, \xi_2), \\ \frac{d\xi_2}{dt} &= b_{10}\xi_1 + b_{01}\xi_2 + b_{20}\xi_1^2 + b_{11}\xi_1\xi_2 + b_{02}\xi_2^2 + b_{30}\xi_1^3 + b_{21}\xi_1^2\xi_2 + b_{03}\xi_2^3 + G^2(\xi_1, \xi_2), \end{aligned} \tag{10}$$

where

$$a_{10} = s - \frac{2s\xi_1^*}{L} - \frac{ab(1+g(\xi_2+\xi_2^*))(\xi_2+\xi_2^*)}{\xi_1^{*2}+a\xi_1^*+ag} + \frac{ab\xi_1^*(2\xi_1^*+a)(1+g(\xi_2+\xi_2^*))(\xi_2+\xi_2^*)}{(\xi_1^{*2}+a\xi_1^*+ag)^2},$$
$$a_{20} = -\frac{2s}{L} + \frac{ab(1+g\xi_2^*)\xi_2^*(3\xi_1^*+a)}{(\xi_1^{*2}+a\xi_1^*+ag)^2} - \frac{ab\xi_1^*(2\xi_1^*+a)^2(1+g\xi_2^*)\xi_2^*}{(\xi_1^{*2}+a\xi_1^*+ag)^3},$$
$$a_{30} = \frac{ab(1+g(\xi_2+\xi_2^*))(\xi_2+\xi_2^*)}{(\xi_1^{*2}+a\xi_1^*+ag)^2} - \frac{ab(4\xi_1^*+a)(2\xi_1^*+a)(1+g(\xi_2+\xi_2^*))(\xi_2+\xi_2^*)}{(\xi_1^{*2}+a\xi_1^*+ag)^3}$$
$$- \frac{ab\xi_1^*(2\xi_1^*+a)^3(1+g(\xi_2+\xi_2^*))(\xi_2+\xi_2^*)}{(\xi_1^{*2}+a\xi_1^*+ag)^4},$$
$$a_{01} = -\frac{ab\xi_1^*\xi_2^{*2}(1+g\xi_2^*)}{\xi_1^{*2}+a\xi_1^*+ag}, \qquad a_{02} = 0, \qquad a_{03} = 0,$$
$$a_{21} = \frac{ab\xi_1^*(2\xi_1^*+a)(1+g(\xi_2+\xi_2^*))(\xi_2+\xi_2^*)}{(\xi_1^{*2}+a\xi_1^*+ag)^2} + \frac{ab(1+g\xi_2^*)\xi_2^*(3\xi_1^*+a)}{(\xi_1^{*2}+a\xi_1^*+ag)^2}$$
$$- \frac{ab\xi_1^*(2\xi_1^*+a)^2(1+g\xi_2^*)\xi_2^*}{(\xi_1^{*2}+a\xi_1^*+ag)^3}$$
$$b_{10} = \frac{ab\xi_2^*(\xi_1+\xi_1^*)(1+g\xi_2^*)}{(\xi_1+\xi_1^*)^2+a(\xi_1+\xi_1^*)+ag}, \qquad b_{01} = \frac{ab(1+g\xi_2^*)\xi_1^*}{\xi_1^{*2}+a\xi_1^*+ag} + \frac{ab\xi_1^*g}{\xi_1^{*2}+a\xi_1^*+ag} - 1,$$

with $G^1(\xi_1,\xi_2) = \sum a_{ij}\xi_1^i\xi_2^j$ and $G^2(\xi_1,\xi_2) = \sum b_{ij}\xi_1^i\xi_2^j$. As a result, the determinant of Jacobian matrix provides the system's first Lyapunov coefficient σ. We are unable to speculate on the sign of the Lyapunov number σ since its expression is so complex as follows:

$$\sigma = -\frac{3\pi}{2a_{01}\Delta^{\frac{3}{2}}}[(a_{10}b_{10}(a_{11}^2+a_{11}a_{02})a_{02}b_{11}) + a_{10}a_{01}(b_{11}^2+a_{20}b_{11}+a_{11}b_{02})$$
$$+ b_{10}^2(a_{11}a_{02}+2a_{02}b_{20}) - 2a_{10}b_{10}(b_{20}^2-a_{20}a_{02}) - 2a_{10}a_{01}(a_{20}^2-b_{20}b_{02})$$
$$- a_{01}^2(b_{11}b_{20}+2a_{20}b_{20}) + (a_{01}b_{10}-2a_{10}^2)(b_{11}b_{02}-a_{11}a_{20}) - (a_{10}^2$$
$$+ a_{10}b_{10})3(b_{01}b_{03}-a_{01}a_{30}) + 2a_{10}((a_{21}+b_{12})+(b_{10}a_{12}-a_{01}b_{21}))],$$

where Δ represents the Jacobian matrix's determinant. We shall calculate the sign of σ numerically as it is theoretically nearly impossible.

7 Spatio-temporal system

In this section, we extend the system (3) to a spatiotemporal framework by incorporating spatial diffusion based on the system's reaction kinetics. Let the spatial domain be denoted by $\Omega \subset \mathbb{R}^2$ with boundary $\partial\Omega$, such that $\Omega = \Omega \cup \partial\Omega$. The random movement of the prey and predator populations is modeled through diffusion terms, resulting in a coupled reaction–diffusion system. The general form of the spatiotemporal model is given as follows:

$$\frac{\partial\xi_1}{dt} = \phi_1(\xi_1,\xi_2) + D_1\nabla^2\xi_1, \tag{11a}$$

$$\frac{\partial \xi_2}{dt} = \phi_2(\xi_1, \xi_2) + D_2 \nabla^2 \xi_2. \tag{11b}$$

Let the prey and predator densities be denoted by $\xi_1(n,p,t)$ and $\xi_2(n,p,t)$, respectively, where $\nabla^2 \equiv \frac{\partial^2}{\partial n^2} + \frac{\partial^2}{\partial p^2}$ represents the two-dimensional Laplacian operator. The parameters D_1 and D_2 denote the diffusion coefficients of the prey and predator populations, respectively, characterizing the random movement of individuals within the spatial domain. Using the dimensionless reaction kinetics approach described in Section 2, we derive the nondimensional form of the proposed spatiotemporal model as follows:

$$\frac{\partial \xi_1}{dt} = \phi_1(\xi_1, \xi_2) + \nabla^2 \xi_1, \tag{12a}$$

$$\frac{\partial \xi_2}{dt} = \phi_2(\xi_1, \xi_2) + d_1 \nabla^2 \xi_2. \tag{12b}$$

Here, $d_1 = \frac{D_1}{D_2}$ represents the ratio of diffusion coefficients. The spatial variables are made dimensionless as $\bar{n} = \frac{n}{\sqrt{D_1}}$ and $\bar{p} = \frac{p}{\sqrt{D_2}}$. For simplicity, the overscore notation is omitted. In the resulting dimensionless reaction-diffusion system (12), all parameters are positive and nondimensional:

$$\xi_1(n,p,0) \geq 0, \quad \xi_2(n,p,0) \geq 0, \quad (n,p) \in \Omega,$$
$$\frac{\delta \xi_1}{\delta n} = \frac{\delta \xi_2}{\delta p}, \quad (n,p) \in \Omega, \quad t \geq 0.$$

Here, we examine the diffuse instability requirement of model (12) and try to understand how predator collaboration affects potential possibilities for pattern formation.

8 Turing instability

A stable homogenous state of equilibrium changes to an unstable one when there are small-amplitude perturbations in the coupled reaction-diffusion system nonuniform disturbance. Turing instability is now functional, and it fulfils the requirement. Hence we show $\xi_1(n,p,t) = \xi_1^*, \xi_2(n,p,t) = \xi_2^*$ is in a constant, uniform state. It should be noted that ξ_1^* and ξ_2^* relate to stable/unstable nodes/focuses, not saddle points, in the time model (3). The homogeneous steady state is locally asymptotically stable in the temporal model (3) if $A_{11} + A_{22} < 0, A_{11}A_{22} - A_{12}A_{21} > 0$. So given the minimal perturbation

$$\xi_1 = \xi_1^* + \in_1 e^{\lambda t} \cos(K_n n) \cos(K_p p),$$
$$\xi_2 = \xi_1^* + \in_1 e^{\lambda t} \cos(K_n n) \cos(K_p p),$$

is necessary, where λ is the growth impact eigenvalue and $0 < \varepsilon_1, \varepsilon_2 \ll 1$. The wave vector $K_1 = K(K_n, K_p)$ also has a wave-number $K = |k_1|$. The system of solutions is transformed into linear after inserting

$$J(k_1^2) = \begin{bmatrix} A_{11} - K_1^2 - \lambda & A_{12} \\ A_{21} & A_{22} - d_1 k_1^2 - \lambda \end{bmatrix},$$

where A_{11}, A_{12}, A_{21}, and A_{22} are same as the matrix A_3 in the Subsection 4.1 and characteristic equation of the Jacobian matrix is given by

$$\lambda^2 - Tr_{k_1} \lambda + Det_{k_1} = 0.$$

Solving it for the λ gives

$$\lambda(k_1) = \frac{1}{2}(tr_{k_1} \pm \sqrt{tr_{k_1} - 4det_{k_1}}),$$

where

$$TrJ(k_1^2) = A_{11} + A_{22} - k_1^2(1+d_1) \equiv Tr(A_3) - k_1^2(1+d_1),$$
$$DetJ(k_1^2) = (A_{11} - k_1^2)(A_{22} - dk_1^2) - A_{12}A_{21} \equiv dk_1^4 - k_1^2(d_1A_{11} + A_{22}) + Det(A_3).$$

The conditions for Turing instability at the steady state (ξ_1^*, ξ_2^*) are given by

$$A_{11} + A_{22} < 0,$$
$$A_{11}A_{22} - A_{12}A_{21} > 0,$$
$$d_1A_{11} + A_{22} > 2\sqrt{d_1(A_{11}A_{22} - A_{12}A_{21})}.$$

Now, we get the equation of bifurcation Turing curve as follows:

$$d_1A_{11} + A_{22} = 2\sqrt{d_1(A_{11}A_{22} - A_{12}A_{21})}. \tag{13}$$

By solving the equation (13) at $k_1 = K_T$, we get

$$k_T^2 = \frac{d_1A_{11} + A_{22}}{2d_1}. \tag{14}$$

As outlined in Subsection 4.1, given that $A_{22} > 0$, it follows that $A_{11} < 0$ in order for the condition $A_{11} + A_{22} < 0$ to hold under certain parametric restrictions. Furthermore, to guarantee that $k_1^2 = k_T^2$ remains positive at the Turing bifurcation threshold, the term $dA_{11} + A_{22} > 0$ must hold. This, in turn, implies that $d_1 < 1$ in order to satisfy the conditions for Turing instability. Consequently, the self-diffusion coefficient for the predator population is lower than that of the prey population in model (12). This result is not limited to a specific functional response, but rather holds for a class of prey-dependent functional responses that incorporate hunting cooperation. This is a critical aspect of spatio-temporal prey-predator models involving cooperative hunting, as in most cases, the self-diffusivity of prey is typically greater than that of predators. This suggests that, on average, predators move faster than their prey. When hunting cooperation is incorporated, the Turing instability conditions are satisfied, and the general expectation that $d_1 > 1$ is revised. In this framework, the rate of movement (diffusivity) of the prey population within a given domain is higher than that of the predators. This can be understood by considering that the prey are actively moving in search of food while also attempting to maintain a safe distance from the predators. In contrast, predators, who are hunting cooperatively, move in packs, resulting in a lower overall diffusion rate. This does not impact their prey-catching efficiency, as their cooperative hunting behaviour compensates for the reduced individual speed. It is important to note that, in the absence of cooperative hunting, predators would need to move faster than the prey to effectively capture them. However, the formation of stationary predator patches requires that the predators move more slowly when cooperating during hunting. To gain a more detailed understanding of this phenomenon, numerical simulation results should be considered. For a diffusion ratio $d_1 < 1$, a Turing instability may occur, and the corresponding critical wavenumber k_T satisfies the relation:

$$k_T^2 = \frac{\det(J_{E_1})}{d}, \quad \text{with } d_1 > 0.$$

The wavelength at the Turing bifurcation threshold is given by

$$\lambda = \frac{2\pi}{k_m},$$

where k_m is the wavenumber corresponding to the maximum real part of the positive eigenvalue of the linearized system.

If the necessary condition is satisfied and the minimum value of k_1^2 becomes negative within a specific range, a Turing instability may arise. Specifically, instability occurs when there exists a value of k_1^2 within the interval:

$$k_1^2 \in (\frac{dA_{11} + A_{22} - \sqrt{(dA_{11} + A_{22})^2 - 4d\det(J_{A_3})}}{2d}, \\ \frac{dA_{11} + A_{22} + \sqrt{(dA_{11} + A_{22})^2 - 4d\det(J_{A_3})}}{2d}).$$

If this condition holds, then the homogeneous steady state $E_3(\xi_1^*, \xi_2^*)$ is unstable with respect to the reaction-diffusion model defined by (12). In summary, the emergence of spatial patterns through diffusion-driven instability is governed by the above criteria, and the onset of a Turing instability can be described within this analytical framework.

9 Numerical simulation

We have derived analytical formulations for spiral and target solutions from the linear amplitude equations (12). To support these findings, we present numerical simulations using the forward Euler method combined with a Laplacian discretization of the coupled reaction-diffusion system with no-flux boundary conditions. Simulations are performed on a two-dimensional grid of size 1×200, with grid spacings $\Delta n = 1$ and $\Delta p = 0.0012$, and a time step of $\Delta t = 0.01$.

To illustrate the dynamics, we first consider the parameter set $L = 0.81, a = 3.15, b = 1, g = 1.78, d = 0.11, s = 1.94$. In this case, $f(\xi_1) = 0$ has two positive roots, and only $(0.6727, 0.2031)$ corresponds to an interior steady state, as shown in Figure 2a. With a second parameter set $L = 0.8, a = 3.1, b = 1, g = 1.7, d = 0.1, s = 1.75$, two coexistence equilibria emerge: $(0.38845, 0.34594)$ and $(0.4987, 0.3586)$, corresponding to the non-negative steady states of system (3), depicted in Figure 2b.

Additionally, we find equilibria $(0.000848, 0.0000585)$ and $(0.4239, 0.0281)$ for the parameter set $s = 0.069, L = 10.569, b = 2.181, g = 0.09, a = 0.358, d = 0.001$. Now, we can solve system (12) for numerical simulatioon of spiral pattern by setting following initial conditions:

$$\xi_1(n, p, 0) = \begin{cases} \xi_1^* + \varepsilon(\xi_1 - 1200)(\xi_2 - 2800), & (\xi_1 - 100)^2 + (\xi_2 - 50)^2 < 200 \\ \xi_1^*, & \text{otherwise} \end{cases} \tag{15a}$$

$$\xi_2(n, p, 0) = \begin{cases} \xi_2^* + \varepsilon(\xi_1 - 1200)(\xi_2 - 2800), & (\xi_1 - 150)^2 + (\xi_2 - 100)^2 < 200 \\ \xi_2^*, & \text{otherwise} \end{cases} \tag{15b}$$

Figure 3 displays stability regions with red, yellow, and blue representing unstable, saddle, and stable regions, respectively. For $L = 3.695, s = 0.896, b = 28.269, a = 0.369, d = 17.952$, and varying g

$(0.089, 0.001, 0.00001$ in panels a-c), the saddle region expands or contracts with changes in g. Similarly, for $L = 3.695, s = 0.896, b = 28.269, a = 0.369, g = 0.009$ and $d = 5.952$, reducing d increases the stable region.

In this Figure 4 shows the global stability of the system (2) using the same parametric values are $s = 0.896, L = 3.695, d = 0.009, a = 0.369$, $b = 21.269, g = 17.952$. It shows that the Lyapunov function is positive and that its time derivative is negative, as demonstrated in Theorem 2.

In Figure 5, the black, green, blue, and purple curves represent the stable, unstable, limit point, and Hopf bifurcation curves, respectively. In Figures 5a and 5b, the points labeled H and GH correspond to the Hopf and generalized Hopf bifurcation points, respectively. In the Hopf bifurcation diagram shown in Figure 5c, the green curve denotes the stable region, indicating that the Hopf bifurcation between the parameter g and the prey–predator population is stable.

Figure 6 presents the numerical results corresponding to the parameter values in Table 3. Figure 6a shows an unstable limit cycle in the time series. Increasing the parameter g stabilizes both prey and predator populations, as illustrated in Figure 6d. Similarly, syatem stabilization is observed with an increase b as shown in Figure 6d.

Figure 7 shows time series of prey and predator populations exhibiting oscillatory behavior. Population peaks alternate, consistent with ecological intuition: prey increase $\rightarrow$ predator increase (with delay) $\rightarrow$ prey decrease $\rightarrow$ predator decrease. The predator curve lags behind the prey, characteristic of predator-prey dynamics. Oscillations appear sustained, suggesting either a non-dissipative system or a short simulation time.

The dynamic behavior of the prey–predator system under different conditions is illustrated in Figures 8 and 9. In Figure 8, the system exhibits a non-constant steady state, where both prey and predator populations oscillate rather than settling at a fixed equilibrium. As the diffusion coefficient d_1 increases from very small values up to 1, the spatial distribution of populations remains irregular, indicating persistent instability. In contrast, Figure 9 shows that at higher diffusion $d_1 = 5$, the system stabilizes, and both populations converge to a steady state. This suggests that increased diffusion, which enhances mixing between species, reduces spatial fluctuations and promotes equilibrium in population densities.

Spatial patterns are explored in Figures 10 and 11. Initial disturbances across the domain generate patterns over time. Within approximately five days, populations spread throughout the area, leaving some regions with fewer predators. Over longer durations (up to 500 days), high population densities persist near domain boundaries, while predator presence remains in the core.

Figure 10 presents the spatial distribution of prey and predator populations. Prey densities are visualized with contour lines overlaid on a heatmap, revealing patchy distributions with high-density regions in yellow/red and low-density regions in blue. Predator populations show similar patchiness, but with lower overall density. Overlapping contours indicate predator-prey proximity, reflecting predator influence on prey distribution.

Figure 11 further illustrates spatial heterogeneity. Predator densities range from 3.345886×10^{-5} (blue) to 3.345906×10^{-5} (red), with higher concentrations in the lower-left quadrant. Prey densities range from 2×10^{-32} to 1.4×10^{-31}, clustering in the upper-left and lower-left regions. These patterns suggest spatial refuges and avoidance behavior by prey, while predators track prey movement. The contrast between fragmented predator distributions and broader prey clusters is consistent with Turing-type instabilities arising from differing diffusion rates.

Overall, these simulations demonstrate the importance of spatial structure in predator-prey systems. Reaction-diffusion dynamics generate diverse patterns, highlighting ecological processes such as pursuit,

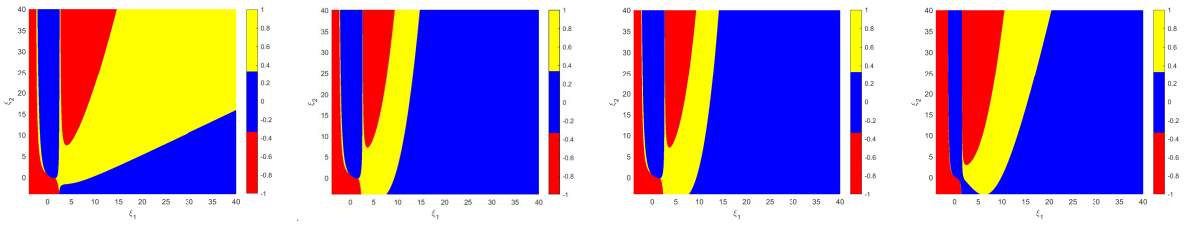

(a) **(b)** **(c)** **(d)**

Figure 3: Bassin of attraction for both prey and predator population for system (3)

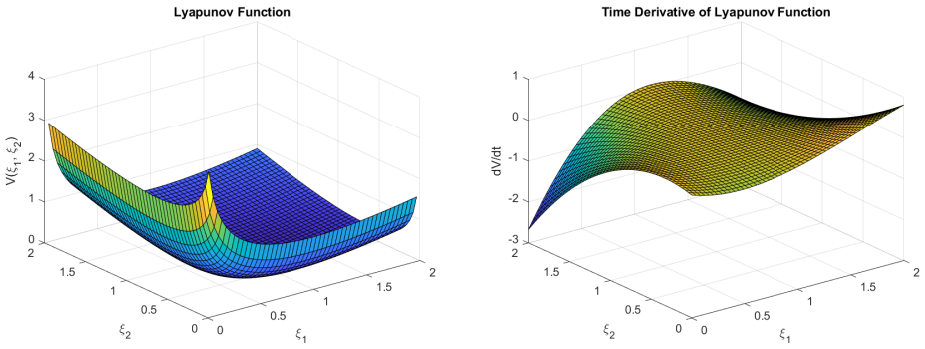

(a) **(b)**

Figure 4: The diagram illustrates the global stability of the system (3).

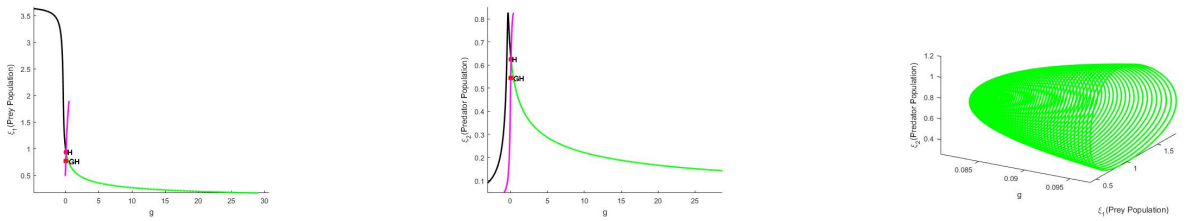

(a) **(b)** **(c)**

Figure 5: The diagram depicts the bifurcation figure between the parameters and the prey and predator populations. The parametric values are $s = 0.896, L = 3.695, d = 0.009, a = 0.369$, $b = 21.269, g = 17.952$.

avoidance, and localized refuges. Spatial heterogeneity plays a critical role in species coexistence, long-term persistence, and the impact of mobility on ecological interactions.

Table 3: Parameters values for Figure 6 are $s = 0.896, L = 3.695, d = 0.009, a = 0.369$

Numerical values of the variable	Steady point	Figure no.
$b = 17.269, g = 7.952$	(0.5342344851, 0.4094659226)	6a
$b = 17.269, g = 11.952$	(0.8503280596, 0.5865597609)	6b
$b = 17.269, g = 17.952$	(1.436287906, 0.7866760849)	6c
$b = 21.269, g = 17.952$	(1.017856282, 0.6607721259)	6d

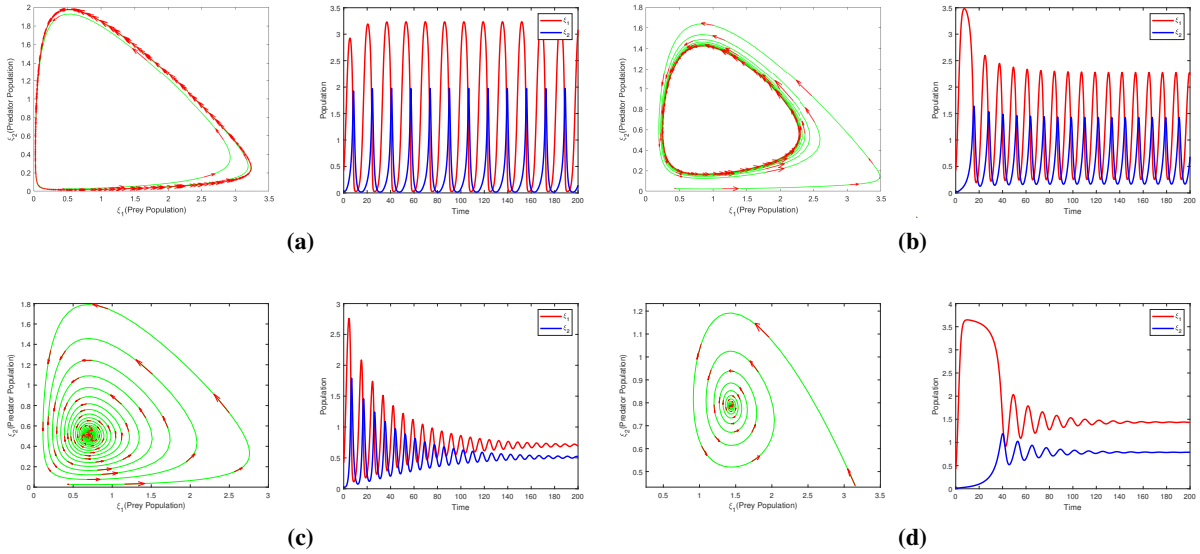

Figure 6: Limit cycle with the time series of system (3)

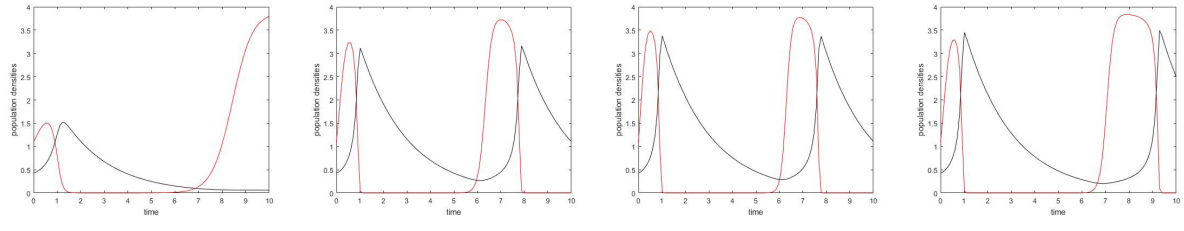

Figure 7: The diagram depicts the time series by changing the parameter of values as follows: (a) to (e) as s, (f) as g with constant time $t = 10$ of the system (12). For $a = 3.6995, L = 3.9185, d = 3.182, s = 8.1883, b = 1.813, t = 10, d_1 = 0.0001$ and (a) the value of $g = 2.3824$, (b)$g = 7.382$, (e) $g = 9.482$. For $a = 3.6997, L = 3.9186, d = 3.282, s = 7.4723, b = 1.813$ (f), the value of $g = 7.1885$ are represented on the graph by the prey-predator population in red and black, respectively.

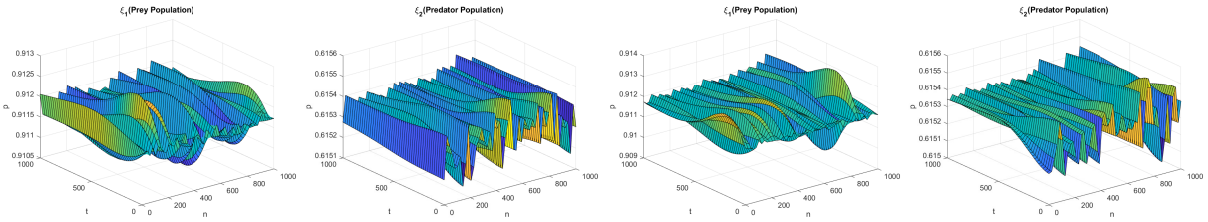

(a) $d_1 = 0.0001$ **(b)** $d_1 = 0.0001$ **(c)** $d_1 = 1$ **(d)** $d_1 = 1$

Figure 8: A non-constant steady state system (12) $s = 0.896, L = 3.695, b = 28.269, g = 0.009, a = 0.369, d = 22.752$

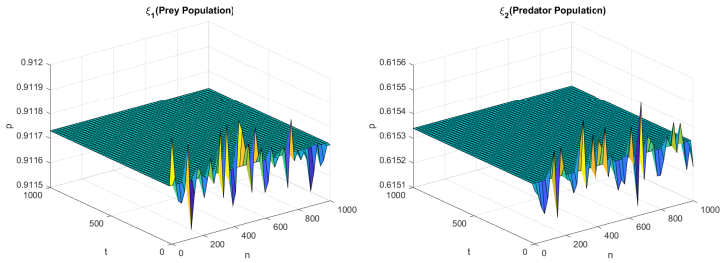

(a) $d_1 = 5$ **(b)** $d_1 = 5$

Figure 9: At $d_1 = 5$, the diagram shows the stable behaviour of the system (12) and the parameter values same as Figure 8.

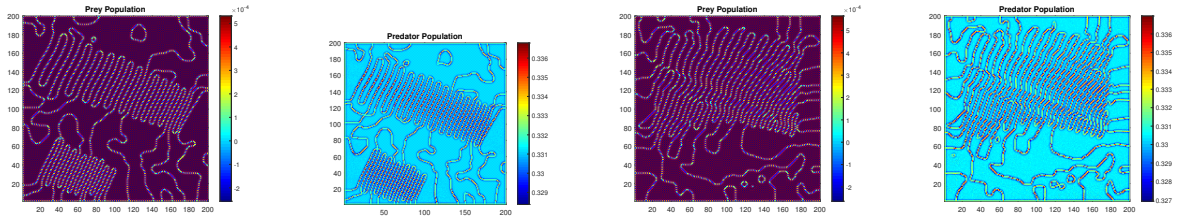

(a) **(b)**

Figure 10: Depicts the effects of b on the models used. We get the strip pattern formations with the other values of parameters fixed. For $M = 700, s = 0.0009, L = 15.369, b = 1.359, a = 1.768, d = 0.001, d_1 = 0.000001, dt = 0.001, dx = \frac{1}{8}, \varepsilon = 10^{-11}$ and $(0.4323096062, 0.1471388727)$ equilibrium point, with change the parameter g as follows: (a) $g = 3.496$, (b) $g = 3.528$.

10 Discussion and conclusion

This study investigates the impact of cooperative predation on the emergence and evolution of spatiotemporal patterns in predator–prey systems. Using both analytical and numerical methods, we demonstrate that stable spatial patterns can develop when predator diffusivity is significantly lower than that of the prey. These findings apply to a broad class of parameterized systems, including reaction–diffusion mod-

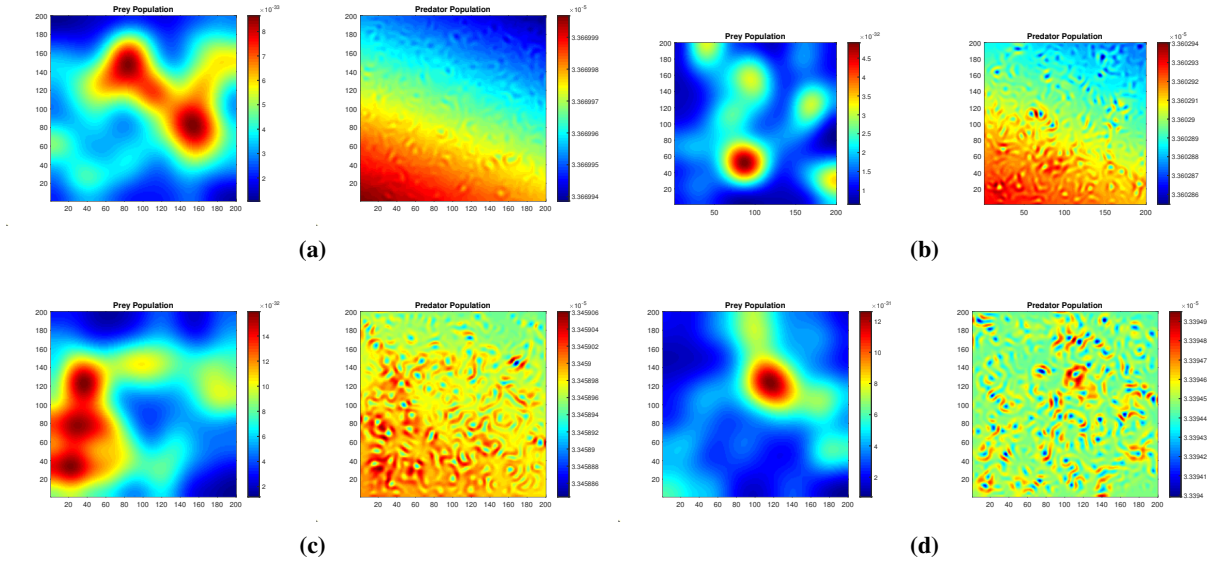

Figure 11: This diagram depicts the Turing patterns changing the values of b with the other parameter values staying the same, showing the effect of b on the model and the spot and strip pattern creation that occurs. For $M = 1000, s = 0.1699, L = 10.369, b = 1.359, a = 5.468, d = 0.01, d_1 = 0.000001, dt = 0.01, dx = 0.25, \varepsilon = 10^{-11}$ and $(0.4323096062, 0.1471388727)$ equilibrium point, with change the parameter b as follows: (a) the value of $g = 2.682$, (b) $g = 2.696$, (c) $g = 2.728$, (d) $g = 2.742$.

els originally developed for chemical processes. To explore this, we consider prey-dependent functional responses that vary with prey density, including forms that exhibit saturation at high prey concentrations. Such functional responses are crucial for modeling cooperative predator behavior and understanding its role in pattern formation.

Our analysis begins by identifying the conditions for local asymptotic stability and Hopf bifurcations in the temporal system. We then extend the model spatially to examine the emergence of distinct spatial structures—such as stripes, spots, and mixed formations—through numerical simulations. The onset of Turing instability is derived analytically, and simulations confirm the conditions under which spatially heterogeneous patterns appear. Without cooperative predation, the model fails to produce Turing-type patterns under biologically realistic parameters. In contrast, when predator cooperation is included, spatial patterns arise from the interaction between limited predator mobility and the faster diffusion of prey. This diffusion imbalance promotes spatial separation, enabling stable coexistence between species.

Under cooperative hunting, areas of high prey density correspond to regions of lower predator density, and vice versa. This inverse relationship reflects an adaptive behavioral response: predators aggregate strategically to optimize hunting success while avoiding overexploitation of prey-rich areas. The model demonstrates that diverse spatial structures—including spots, stripes, and maze-like formations—can emerge when parameters favor unlimited resource access and high functional responsiveness. Although temporal bifurcations may also occur, realistic spatiotemporal dynamics depend strongly on initial conditions and feedback mechanisms within the system. Even when patterns appear static, they are maintained by continuous dynamic interactions as predator and prey populations fluctuate over time. Predators track prey movements across the landscape, contributing to the observed spatiotemporal com-

plexity.

From an ecological perspective, cooperative predation enhances the long-term stability of predator–prey coexistence. Group hunting behaviors have been documented in species such as wolves, lions, hyenas, chimpanzees, jackals, and cheetahs, where predation efficiency tends to saturate with increasing group size. Predators typically occupy regions adjacent to prey-rich zones, improving hunting efficiency while minimizing competition. Simulations indicate that predators and prey often occupy distinct but adjacent regions, enabling effective predation without direct overlap. By positioning themselves at the periphery of prey-dense areas, predators reduce prey detection and escape rates. Over time, predator movements closely mirror prey migrations, maintaining dynamic equilibrium and preventing overexploitation.

In contrast, non-cooperative predation often leads to prey overexploitation and population collapse. In our model, the lower diffusion coefficient of predators ensures spatial constraint, promoting localized and sustainable predation. Cooperative hunting behavior, as supported by ecological theory [9], provides significant advantages in predator–prey dynamics.

Incorporating cooperative predation into predator–prey models greatly enhances their ecological realism and expands their applicability. The analytical and numerical framework developed in this study provides a robust approach for investigating pattern formation in spatially extended ecosystems. Given the scarcity of models that explicitly address group predation within reaction–diffusion frameworks, this work offers novel insights into coordinated hunting dynamics.

Future research could build upon these findings to explore spatial invasion, population persistence, and heterogeneous species distributions. Further studies should also examine the effects of more complex functional responses, such as the Holling type IV response, which accounts for saturation in predation rates. Additionally, incorporating environmental feedback, adaptive foraging strategies, and habitat heterogeneity could reveal new mechanisms driving spatiotemporal pattern formation in natural ecosystems.

Conflict of interest

The authors declare that they have no conflict of interest.

References

[1] M.T. Alves, F.M. Hilker, *Hunting cooperation and Allee effects in predators*, J. Theor. Biol. **419** (2017) 13–22.

[2] M. Banerjee, S. Abbas, *Existence and non-existence of spatial patterns in a ratio-dependent predator-prey model*, Ecol. Complex. **21** (2015) 199–214.

[3] M. Banerjee, S. Ghorai, N. Mukherjee, *Approximated Spiral and Target Patterns*, Unpublished manuscript, 2017.

[4] A. Batabyal, D. Jana, *Significance of additional food to mutually interfering*, Unpublished manuscript, 2020.

[5] D.S. Cohen, J.C. Neu, R.R. Rosales, *Rotating spiral wave solutions of reaction-diffusion equations*, SIAM J. Appl. Math. **35** (1978) 536–547.

[6] R.F. Cui, Q.H. Chen, J.X. Chen, *Separation of nanoparticles via surfing on chemical wavefronts*, Nanoscale **12** (2020) 12275–12280.

[7] E. Goodale, G. Beauchamp, G.D. Ruxton, *Mixed-Species Groups of Animals: Behavior, Community Structure, and Conservation*, Elsevier, 2017.

[8] G.J. Jayalakshmi, A. Tamilselvan, *Second order difference scheme for singularly perturbed boundary turning point problems*, J. Math. Model. **9(3)** (2021) 633-643.

[9] S. Kumar, M. Erik, *An observer for an occluded reaction diffusion system with spatially varying parameters*, Chaos **17** (2017).

[10] Y. Kuramoto, T. Yamada, *Pattern formation in oscillatory chemical reactions*, Prog. Theor. Phys. **56** (1976) 724–740.

[11] A.B. Medvinsky, S.V. Petrovskii, I.A. Tikhonova, H. Malchow, B.L. Li, *Spatio-temporal complexity of plankton and fish dynamics*, SIAM Rev. **44** (2002) 311.

[12] H. Mokhtari, L. Rahmani, *Mathematical modeling of the effect of an insulating stiffener on a nonlinear thermo-elastic plate*, J. Math. Model. **9(3)** (2021) 611-631.

[13] N. Mukherjee, M. Banerjee, *Hunting cooperation among slowly diffusing predators can induce stationary Turing pattern*, Phys. A: Stat. Mech. Appl. **599(1)** (2022) 127417.

[14] J. Roy, S. Dey, M. Banerjee, *Maturation delay induced stability enhancement and shift of bifurcation thresholds in a predator–prey model with generalist predator*, Math. Comput. Simul. **211** (2023) 368–393.

[15] S. Rozgonyi, K. Hangos, G. Szederknyi, *Determining the domain of attraction of hybrid non-linear systems using maximal Lyapunov functions*, Kybernetika **46** (2010) 19–37.

[16] M.J. Smith, J.A. Sherratt, N.J. Armstrong, *The effects of obstacle size on periodic travelling waves in oscillatory reaction-diffusion equations*, Proc. R. Soc. A **464**(2008) 365–390.

[17] S. Tapan, J.P. Pallav, B. Malay, *Slow–fast analysis of a modified Leslie–Gower model with Holling type I functional response*, Nonlinear Dyn. **108** (2022) 4531–4555.

[18] A.M. Turing, *The chemical basis of morphogenesis*, Phil. Trans. R. Soc. Lond. B **237** (1952) 37–72.

[19] R.K. Upadhyay, D. Pradhan, R.D. Parshad, P. Roy, *Existence of global attractor in reaction–diffusion model of obesity-induced Alzheimer's disease and its control strategies*, Commun. Nonlinear Sci. Numer. Simul. **140** (2025) 108396.

[20] S. Zawka, D.N.S. Pichika, *Existence and optimal harvesting of two competing species in a polluted environment with pollution reduction effect*, J. Math. Model. **9(3)** (2021) 517-536.